

Wetting and Diffusion of Water on Pristine and Strained Phosphorene

Wei Zhang¹, Chao Ye¹, Lin Bi², Zaixing Yang³, and Ruhong Zhou^{2,3,4}

¹*Bio-X Lab, Department of Physics, and Soft Matter Research Center, Zhejiang University, Hangzhou 310027, China*

²*Computational Biology Center, IBM Thomas J. Watson Research Center, Yorktown Heights, NY 10598, USA*

³*Institute of Quantitative Biology and Medicine, SRMP and RAD-X,
Collaborative Innovation Center of Radiation Medicine of Jiangsu Higher
Education Institutions, Soochow University, Suzhou 215123, China*

⁴*Department of Chemistry, Columbia University, NY 10027, USA*

(Dated: August 24, 2018)

Phosphorene, a newly fabricated two-dimensional (2D) nanomaterial, have exhibited promising application prospect in biology. Nonetheless, the wetting and diffusive properties of bio-fluids on phosphorene are still elusive. In this study, using molecular dynamics (MD) simulations, we investigated the structural and dynamic properties of water on pristine and strained phosphorene. The MD simulations illustrated that the diffusion of water molecules on the phosphorene surface is anisotropic, while strain-enhanced diffusion is clearly present which arises from strain-induced smooth of the energy landscape. The contact angle of water droplet on phosphorene exhibited a nonmonotonic variation with the transverse strain. The structure of water on transverse stretched phosphorene was demonstrated to be different from that on longitudinal stretched phosphorene. Moreover, we discovered that the contact angle of water on strained phosphorene is proportional to the quotient of longitudinal and transverse diffusion coefficients of interfacial water. These findings would offer helpful insights in potential ways of manipulating the wetting and transport of water at nanoscale, and in future bio-applications of phosphorene.

Keywords: pristine/strained phosphorene, contact angle, diffusion coefficient, molecular dynamics

I. INTRODUCTION

As a newly fabricated 2D nanomaterial composed of phosphorus atoms, phosphorene possesses a direct band gap which makes it a natural semiconducting nanomaterial [1, 2]. The specific properties of phosphorene has made its potential applications in biology possible [3–5]. Notably, using a few layers of phosphorene, researchers have successfully fabricated the field-effect transistor [6, 7], which is a desirable device for biodetection and biosensing [8–10]. Compared to graphene, phosphorene is more biological friendly due to its less disruption to proteins [4]. Moreover, as photothermal agents, black phosphorus (multiple layers of phosphorene) quantum dots have exhibited excellent performances in killing C6 and MCF7 cancer cells [5]. Extensive bio-applications of this nanomaterial need more insights in the wetting and diffusive properties of bio-fluids in contact with the phosphorene.

The structure and dynamics of interfacial water at various nanomaterial surfaces are of fundamental importance for developing nanomaterials potential applications in biology and nanofluidics. The structure of water is perturbed heavily near surfaces which have the potential to affect water diffusion [11, 12] and proteins adsorption [13]. During recent years, the wetting and diffusive properties of water in contact with two-dimensional (2D) nanomaterials, such as graphene [14–18], boron-nitride sheets [14, 19, 20], WS₂ and MoS₂ [21, 22] etc., have been widely examined. These studies have strongly promoted applications of these 2D nanomaterials in biology and nanofluidics. The structure and dynamic of water on phosphorene, a new member of 2D nanomaterials, are

still elusive.

Another promising aspect of phosphorene is its great mechanical flexibility [23], due to the hexagonally arranged phosphorus atoms and the subsequently formed puckered honeycomb structure inside the monolayer of phosphorene. A computational result based on first-principles showed that single-layer phosphorene could actualize tensile strain up to ~ 0.5 [24]. It has also been demonstrated that the electrical [25–28], optical [29, 30], thermoelectric [31–33] and mechanical [24, 26, 34] properties of phosphorene could be modified upon mechanical strain. The puckered structure of phosphorene brings anisotropy and negative Poisson ratio [24, 31]. The strain also gives rise to phosphorene’s transition between metal and semiconductors [28, 31, 34]. Therefore, what kind of changes in the structure and dynamics of water on strained phosphorene would occur are naturally topics of interest.

In this study, using molecular dynamics (MD) simulations, we measured the contact angle, diffusion coefficient and distribution of water on pristine and strained phosphorene. We found that the diffusion of water molecules at the surface of phosphorene is anisotropic, and strain-enhanced water diffusion is clearly present. The structure and wetting of water on transverse stretched phosphorene differs from that on longitudinal stretched one. The contact angle of water droplet nonmonotonously changes with the transverse strain, but it nearly linearly changes with the longitudinal strain. Also, the distribution of water near the surface of phosphorene exhibited obvious changes when the transverse strain increased, while the distribution of water barely changed when the longitudinal strain was imposed on phosphorene. Additionally, we

found that the contact angle of water on strained phosphorene is proportional to the quotient of longitudinal and transverse diffusion coefficients of interfacial water. The dispersion energy and free energy profile of water were calculated to interpret the above phenomena.

II. METHODS

MD simulations were performed to generate strained phosphorene, as well as to explore the wetting and diffusive properties of water on pristine and strained phosphorene. The Gromacs package 4.5.7 [35] and OPLS-AA force field [36] were used for the simulations. The SPC/E model was used to model water molecules. Phosphorene with a dimension of $156 \text{ \AA} \times 173 \text{ \AA}$ was chosen for this study. The phosphorus atoms were modeled as uncharged Lennard-Jones particles. The depth of potential well ε_{pp} , cross sections σ_{pp} and bond strength constants are set at $0.400 \text{ kcal mol}^{-1}$, 3.33 \AA and $297 \text{ kcal mol}^{-1} \text{ \AA}^{-2}$ [37], respectively.

Using the pulling code of Gromacs, we produced phosphorene under various strain conditions. Note that the strain being discussed in this study only refers to tensile strain. Phosphorene was therefore stretched along two typical direction: transverse (perpendicular to the pucker) and longitudinal (parallel to the pucker), as shown in Fig.1(a). Phosphorene with strain $\varepsilon = 0$ corresponds to the pristine phosphorene. Figure S1 in the Supporting Information shows four representative configurations of strained phosphorene. The initial water droplet which was configured as a cubic and consists of 2828 molecules was set onto phosphorene under various strain condition. During the first few nanoseconds of the simulation, the water droplet gradually converted from a cubic into a hemisphere, as illustrated in Fig. 1(b). We chose 10 morphologies of phosphorene with different degrees of transverse strain, as well as other 10 phosphorene morphologies with different degrees of longitudinal strain for the interaction with water droplet. Each phosphorene-water system was simulated for 16 ns, and the trajectory of the last 1 ns was extracted for further analysis. The strained phosphorene was fixed throughout the simulation. The particle-mesh Ewald method [38] with a grid spacing of 1.2 \AA was applied to simulate the long-range electrostatic interactions, and a typical cut-off 10 \AA was applied for the van der Waals interactions. All simulations were performed in an NVT ensemble at a constant temperature of 298 K by using v-rescale thermostat [39].

The water contact angle θ was measured by fitting the time-averaged liquid-vapor interface [40]. The liquid-vapor interface is defined as the contour with half of the bulk density, while the number density of water droplet was calculated by the time-averaged spatial mesh with a grid spacing of 0.5 \AA . The liquid-vapor interface was then fitted into an arc, while θ was calculated as the angle of contingence at the liquid-solid interface (refer to Figure

S2 in the Supporting Information).

III. RESULTS

The Young's modulus of phosphorene is sensitive to directions upon which strains were imposed, due to the nanomaterial's anisotropic nature. Figure S3 in Supporting Information illustrates the relationship between the strain at transverse and longitudinal directions and the pull force exerted along these directions. The slope of transverse strain as a function of pull force is clearly steeper than that of longitudinal strain, indicating less stiffness in phosphorene when stretched in the transverse direction. These results consist with previous calculations based upon first-principles density functional theory [23, 24].

The strains imposed upon the nanomaterial affect not only phosphorene's electronic and mechanical properties, but the contact angle of water droplet on phosphorene as well. As shown in Fig. 1(c), the strains exerted in different directions have a distinct effect on the contact angle θ . An increase of the transverse strain ε_T causes θ to first increase, and then decrease after the peak is reached. At $\varepsilon_T \sim 0.3$, we observed the maximal contact angle θ_{max} . However, for strains imposed upon the longitudinal direction, the relationship between θ and longitudinal strain rate ε_L is clearly monotonic. A comparison between contact angles of water droplet on phosphorene under different directional strains also showed an overall larger contact angles under transverse than longitudinal strains.

Along with the differences in water contact angles, the transverse and longitudinal strains also cause different deformations of the phosphorene surface. While strain in the transverse direction effectively flattens the pucker of phosphorene, longitudinal strain, however, has little effect on the bending structure of the pucker ring. The distinct deformation of the monolayer of phosphorene leads to different interactions between water droplet and phosphorene. Figure S4 in Supporting Information illustrates the interaction energy E_{WS} between water droplet and the substrate phosphorene as a function of the strain along transverse and longitudinal directions. The energy curves exhibit similarity to that of the contact angle as shown in Fig. 1(c). Due to this similarity, we examined the relationship between θ and E_{WS} by fitting the former with the latter variable. As shown in Fig. S5, there is a clear linear relationship between the two variables, thus inferring a major influence upon the water contact angle by the interactions between water droplets and the substrate.

The contact angle θ nonmonotonically changes with the transverse strain, which is primarily caused by non-monotonic variations of the interaction energy E_{WS} . To analyze the influences of the transverse strain on E_{WS} in detail, we calculate the interaction energy between water droplet and phosphorous atoms in bottom E_{WS}^B and up-

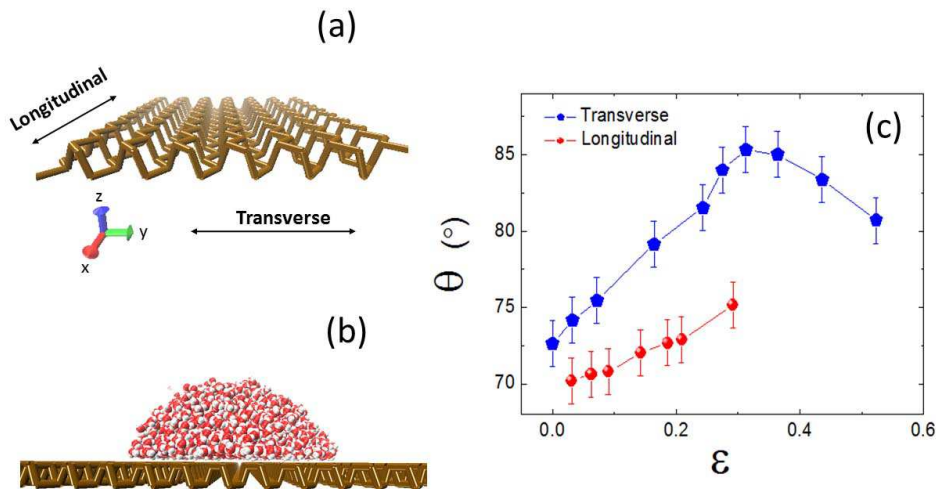


FIG. 1: (a) Perspective view of transverse and longitudinal directions upon which strains were imposed. (b) A snapshot of water droplet on phosphorene ($\epsilon = 0$) in the end of the MD simulation. (c) The water contact angle θ as a function of the transverse and longitudinal strain.

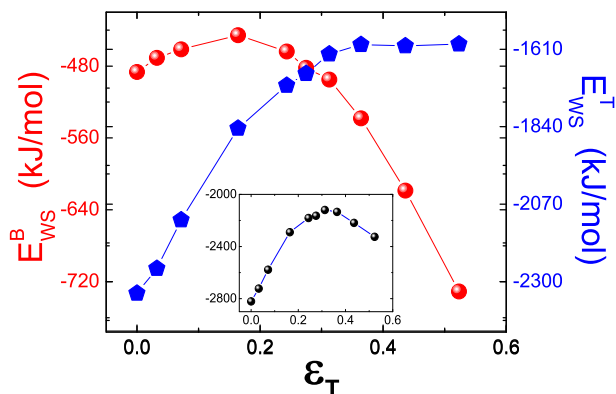


FIG. 2: The interaction energy between water droplet and phosphorous atoms in bottom (E_{WS}^B red circles) and upper (E_{WS}^T blue pentagons) surface of the puckered surface of phosphorene as a function of the strain along transverse direction. The inset shows the combined interaction energy $E_{WS} = E_{WS}^B + E_{WS}^T$.

per E_{WS}^T surfaces of the puckered monolayer of phosphorene, respectively (see Fig. 2). Here $E_{WS} = E_{WS}^B + E_{WS}^T$. With the increase of the transverse strain ϵ_T , the density of atoms in upper surface decreases, thus E_{WS}^T weakens remarkably. Meanwhile, the atoms in bottom surface approach the water droplet and its density also decreases. When $\epsilon_T < \sim 0.16$, the decrease of the density of atoms in bottom surface dominates the interaction, and E_{WS}^B weakens slightly. While $\epsilon_T > \sim 0.16$, however, the approach of atoms in bottom surface dominates the inter-

action, and E_{WS}^B enhances dramatically. The combined interaction effect of upper and bottom surface atoms with water droplet is that as increasing ϵ_T the interaction energy E_{WS} increases firstly and then decreases after ϵ_T reaches ~ 0.3 , as shown in the inset of Fig. 2.

In addition to water contact angle, the strain may also affect the structure of water near phosphorene. In order to understand the structure of interfacial water molecules, we measured the density distribution function (DDF) of oxygen atoms along the direction normal to the surface (z axis). DDF $g(z)$ is defined as in Equation (1):

$$g(z) = \rho(z)/\bar{\rho}, \quad (1)$$

where $\rho(z)$ is the density of oxygen atoms within a thin slice of height z parallel to the surface (the thickness of the slice is set at 0.2 \AA), and $\bar{\rho}$ is the mean density of oxygen atoms in the bulk area. Note that the zero point of z corresponds to the geometric center of phosphorene in z axis direction. An equilibrium system consisting of 25662 water molecules, as shown in Fig. 3(a), was used to study the density distribution and diffusion of water molecules. Figure 3(b) and (c) exhibited $g(z)$ of oxygen atoms near phosphorene under various transverse and longitudinal strains. Due to the dispersive interaction between phosphorous atoms and water molecules, the structure of water near phosphorene is considerably affected and shows double peak character. The double peaks of $g(z)$ in both Fig. 3(b) and (c) indicate the two-layer structure of water in the vicinity of phosphorene, with the first peak corresponding to the first layer of water. The density of oxygen atoms in the first water layer can be 2.8 times larger than that in the bulk. While $z > \sim 1.0 \text{ nm}$, the density fluctuation disappears and the bulk density is recovered. Meanwhile, the difference between Fig. 3(b) and (c) is worth noting. In Fig. 3(b),

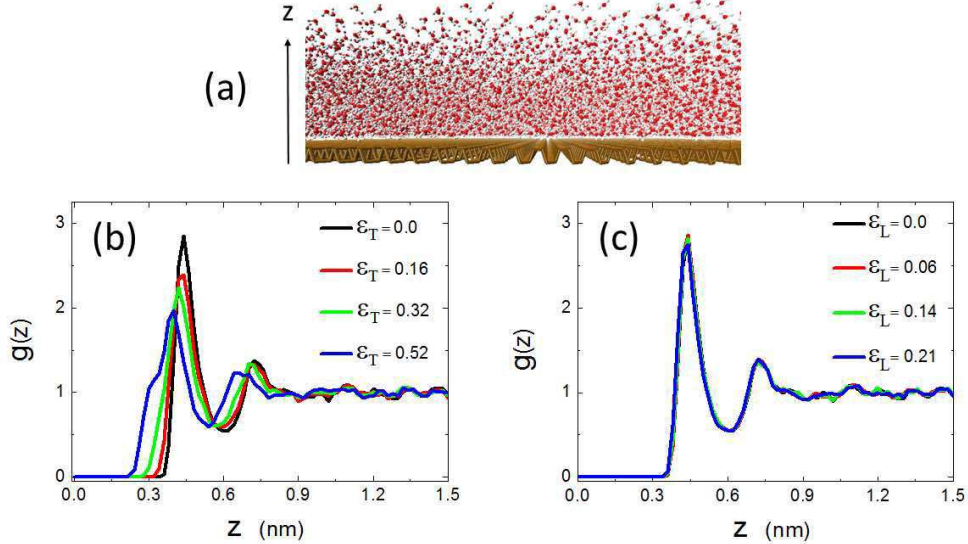


FIG. 3: (a) A snapshot of the simulation system for studying the density distribution and diffusion of water molecules. (b) and (c) The density distribution function of oxygen atoms $g(z)$ as a function of the distance z under different magnitudes of strains.

TABLE I: The critical position z_c , the height g_{max} and half-width W of the first peak of the density distribution function (DDF) of oxygen atoms corresponding to various values of the transverse strain ϵ_T .

ϵ_T	z_c (nm)	g_{max}	W (nm)
0	0.36	2.85	0.08
0.03	0.35	2.68	0.10
0.07	0.34	2.64	0.10
0.16	0.32	2.38	0.10
0.24	0.30	2.26	0.12
0.28	0.30	2.21	0.12
0.31	0.28	2.24	0.12
0.36	0.25	2.14	0.14
0.43	0.24	2.08	0.15
0.52	0.22	1.97	0.18

as transverse strain increases, both the critical position z_c where oxygen atoms appear, as well as the maximal DDF g_{max} decreases, but the half-width of the first peak W increases (see Table 1). On the other hand, the longitudinal strain showed almost no effect on $g(z)$, as shown in Fig. 3(c).

The above results demonstrated that the effects of transverse and longitudinal strain on the static structure of interfacial water are distinct, which can be partly attributed to the anisotropic mechanical properties of phosphorene. In the following discussion, we present the effects of the strain on the dynamic properties of interfacial water.

In order to examine the dynamic properties of liquid on phosphorene, we begin with the self-diffusion of water

molecules, since it is considered to be the most representative dynamic property of liquid upon nanomaterials. The transverse and longitudinal self-diffusion coefficients D_T and D_L are derived from the following equations:

$$\begin{aligned}
 D_T &= \frac{1}{2N\tau} \sum_i \langle |y_i(t+\tau) - y_i(t)|^2 \rangle_t, \\
 D_L &= \frac{1}{2N\tau} \sum_i \langle |x_i(t+\tau) - x_i(t)|^2 \rangle_t,
 \end{aligned} \tag{2}$$

where $x_i(t)$ and $y_i(t)$ are the coordinates of the i th water molecule at time t ; τ is the lag time and N is the number of molecules included in this calculation. The angle brackets $\langle \dots \rangle_t$ indicate an averaged calculation over a duration of time t . Figure 4 shows the transverse and longitudinal diffusion coefficient of water molecules near phosphorene with various strain conditions. It is clear from the separation of curves as shown in Fig. 4, that the diffusion of water molecules on pristine phosphorene is anisotropic, mainly due to the puckering surface morphology of phosphorene. Compared to motions in the transverse direction, a higher D_L coefficient indicates that it is much easier for water molecules to move along longitudinal direction. The transverse diffusion coefficient D_T decreases monotonically with increased transverse strain ϵ_T . The longitudinal diffusion coefficient D_L increases while ϵ_T is smaller than 0.16, and decreases after ϵ_T rises above 0.16, as shown in Fig. 4(a) and its inset. The effects of longitudinal strain on the diffusion of interfacial water differ from that of transverse strain. As increasing longitudinal strain ϵ_L , D_T decreases but D_L increases. As shown in Fig. 4(b), D_L increases from

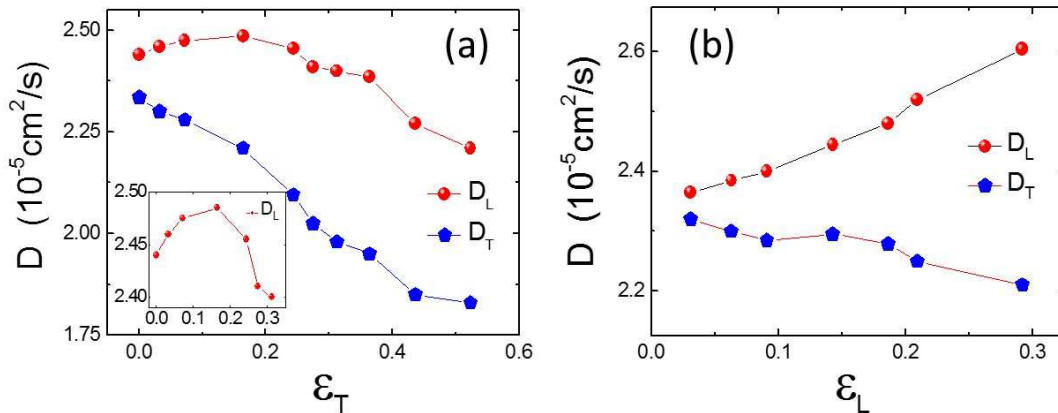


FIG. 4: The diffusion coefficient D of water molecules in the first layer as a function of (a) the transverse and (b) longitudinal strain.

2.37 to 2.61 ($10^{-5} \text{cm}^2/\text{s}$) in the measured range of ε_L . In contrast, the change of D_T is not as significant. Clearly, the effects of ε_T and ε_L on the diffusion of interfacial water are all of an anisotropic manner.

To rationalize the diffusion behaviors of the interfacial water, we computed the free energy profile of water within the first layer $\Delta F(x, y)$ with the equation:

$$\Delta F(x, y) = -k_B T \ln P_o(x, y). \quad (3)$$

Here, $P_o(x, y)$ is the spatial probability distribution function of the oxygen atoms of water within the first layer at coordinate (x, y) . This approach has been previously applied to examine the friction of water on graphene and boron nitride [20]. In Fig. 5, we present $\Delta F(x, y)$ as scaled by $k_B T$ under different transverse strains. The free energy profile $\Delta F(x, y)$ obviously exhibits a grooved trend of phosphorene surface, which is an indication of anisotropy. The coordinate with the minimal value of free energy appears in the region of the groove of phosphorene.

For pristine phosphorene ($\varepsilon_T = 0$ and $\varepsilon_L = 0$), the free energy profile $\Delta F(x, y)$ shows clear "zigzag" pattern in the grooved region (see Fig. 5(a)), which is very similar to famous "swallow gird". The maximal energy barrier for water molecules to translate along longitudinal direction is about $2 k_B T$, while water molecules need to cross energy barrier of $3 k_B T$ to move in transverse direction. It is more difficulty for interfacial water molecules to move in transverse direction compared to longitudinal translation. Thus, the diffusion coefficient of interfacial water along the longitudinal direction is larger than that along the transverse direction.

The strain ε_T acts to broaden the interval of free energy ribbons (low-energy region along the groove) which correspond to groove width of phosphorene. The broadening of free energy ribbon interval constrains the diffusion of water molecules along transverse direction, since it introduces more difficulty in water molecules' crossing

of broadened energy barrier. Meanwhile, the strain ε_T increases the mean energy barrier for water molecules to move in transverse direction, thus hindering the motion of water molecules along the transverse direction. Consequently, the transverse diffusion coefficient D_T decreases as ε_T increases, as shown in Fig. 4(a).

With an increased strain ε_T , the "zigzag" form gradually disappears and the free energy ribbons become smooth (the low-energy region links in line), which is propitious to longitudinal diffusion of water molecules. Thus, the longitudinal diffusion coefficient D_L increases when ε_T is smaller than 0.16, as shown in the inset of Fig. 4(a). While ε_T is larger than 0.16, the effects of phosphorus atoms at the bottom of the groove begin to dominate water's diffusion. As ε_T increases D_L decreases, due to the increased attraction of phosphorus atoms at the bottom of the groove (see Fig. 2).

As for the situations while phosphorene is under longitudinal stretching, the variations of the free energy profile $\Delta F(x, y)$ is different from those while phosphorene is under transverse stretching (see Fig. S6 in Supporting Information). The longitudinal strain ε_L obviously attenuates "zigzag" pattern of free energy ribbon, which accounts for the enhancement of D_L as ε_L increases. However, unlike the effect of ε_T , the longitudinal strain ε_L narrows the groove width, while shows little effect on its depth, which increases mean height of energy barrier but decreases its width. The increased energy barrier constrains the diffusion of water molecules along transverse direction. On the other hand, the decrease of the width of energy barrier is propitious to increase D_T . Under the combined influences of these two factors (the increased height and decreased width of energy barrier), as ε_L increases, the transverse diffusion coefficient D_T decreases slightly.

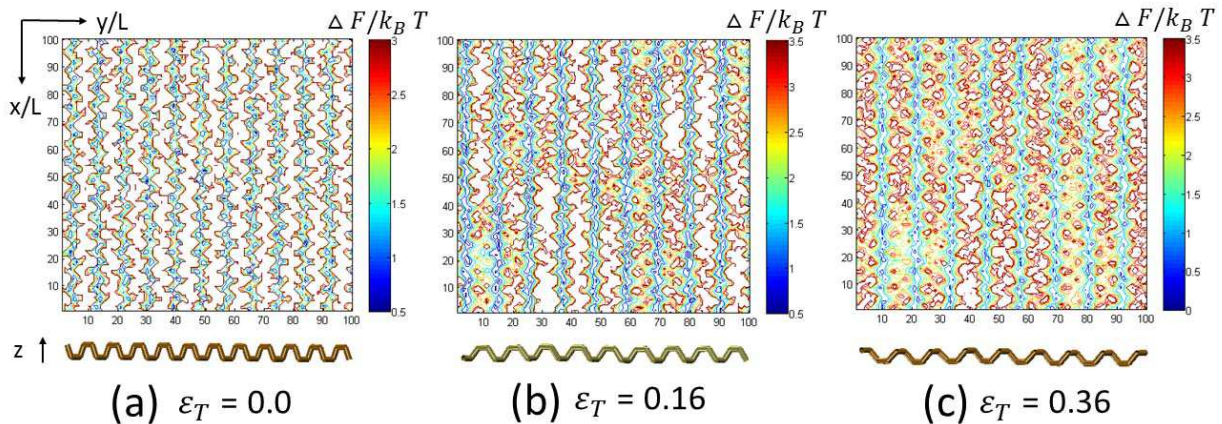


FIG. 5: Free energy profile of water within the first layer $\Delta F(x, y)$ scaled by $k_B T$ for three values of ε_T . Here, the scaling parameter $L = 0.05$ nm.

IV. DISCUSSION

Though the longitudinal strain ε_L obviously smoothes the free energy ribbon and increases the longitudinal diffusion coefficient of interfacial water, it has all most no effects on DDF $g(z)$ (see Fig. 3(c)). The DDF $g(z)$ in Fig. 3(b), however, obviously changes with the transverse strain ε_T , which is caused by the flattening of the puckered surface of phosphorene. The flattening of the surface of phosphorene leads to the decrease of the critical position z_c and the increase of the space interval of free energy ribbon. The increase of the half-width W may derive from the increased ribbon interval. The decrease of the height g_{max} mainly arise from the weakened interaction energy between water and phosphorene. Consequently, DDF $g(z)$ is related not only to the dispersion energy between water and nanomaterials, but also to the distribution of water molecules on nanomaterials' surface.

The quotient D_L/D_T , instead of D_L or D_T per se, exhibits a linear relationship with the contact angle θ of water droplet, as shown in Fig. 6. The variation of the width and depth of the groove of phosphorene caused by the strain directly affects the interaction energy E_{WS} and the free energy profile $\Delta F(x, y)$. The contact angle θ and the diffusion coefficient of water molecules in the first layer are mainly determined by the interaction energy E_{WS} and free energy profile $\Delta F(x, y)$, respectively. The free energy profile $\Delta F(x, y)$ jointly affects the transverse and longitudinal diffusion of water molecules. In this sense, the contact angle θ should be related to the community of the diffusion of water molecules along transverse and longitudinal direction. However at present, we have not yet found a quantitative interpretation regarding the relationship between the ratio D_L/D_T and water contact angle θ , which needs further investigation.

Changing the form of puckering surface of phosphorene by the strain could effectively enhance or attenuate the diffusion of interfacial water molecules, which might

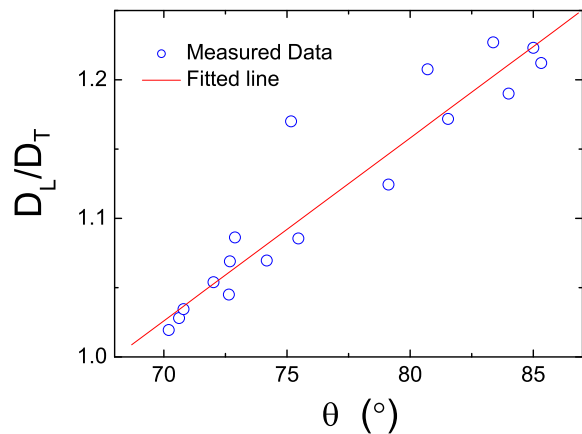


FIG. 6: The quotient of D_L/D_T as a function of the contact angle θ of water droplets. The fitting line has the form: $D_L/D_T = 0.1 + \theta \times 0.013(^{\circ})^{-1}$.

shed light on controlling/designing the motion of interfacial molecules. By controlling the strain, one could construct continuous diffusion (or wetting) gradient, which is of interest in artificial microscopic walk [41, 42]. The anisotropic diffusion of water molecules near phosphorene may also affect phosphorene's motion in complex biological systems, which is of importance for phosphorene's potential bio-applications, such as localized bioprobes and drug delivery.

V. CONCLUSION

In this study, we investigated the wetting and diffusive properties of water near both pristine and strained phosphorene with MD simulations. It was found that the

pristine phosphorene is of weakly hydrophobicity, with a water contact angle of $\sim 72^\circ$. As for the interactions between water droplet and phosphorene under different strain conditions, we discovered that the contact angle θ of water droplets firstly increases, then decreases as the transverse strain reaches the critical threshold of 0.3. However for longitudinal strain, the contact angle θ only increases monotonically as the strain increases. The changes in contact angles are mainly determined by the interaction energy between the water droplet and phosphorene. The structure of the interfacial water dramatically changes with the transverse strain ε_T , but the longitudinal strain ε_L has almost no effect on water's structure.

While the diffusion of water molecules near pristine phosphorene surface is anisotropic, the longitudinal diffusion coefficient D_L is larger than that (D_T) in the transverse direction. As the transverse strain ε_T increases, D_T decreases monotonically, while D_L exhibits an inverted U-shaped curve. The longitudinal strain ε_L , on the other hand, causes D_L to increase, and D_T to decrease monotonically. We also calculated the free energy

profile $\Delta F(x, y)$ so as to determine the main cause of variations in the diffusion of water molecules near phosphorene. It was shown that the smoothing of the energy landscape enhances D_L , and the increased energy barrier makes D_T decrease. Last but not least, we found that the quotient D_L/D_T is positively correlated with the contact angle θ .

As a novel 2D nanomaterial, phosphorene has the potential to be applied extensively in biological systems in the future. It is hence necessary to investigate the wetting and diffusive properties of water on both pristine and strained phosphorene, so as to shed light on possible applications. Our study would potentially help with understanding and manipulating the wetting and diffusive properties of liquid on phosphorene, which is critical for phosphorene's application in the fields of biology and nanofluidics.

Acknowledgments: This research is supported in part by the National Natural Science Foundation of China (Grant Nos. 11574268, 11504032, and 11474054), and China Postdoctoral Science Foundation (Grant Nos. 2015T80610 and 2014M560473).

-
- [1] Lu W, Nan H, Hong J, Chen Y, Zhu C, Liang Z, et al. Plasma-assisted fabrication of monolayer phosphorene and its Raman characterization. *Nano Research*. 2014;7:853-9.
- [2] Liu H, Du Y, Deng Y, Ye PD. Semiconducting black phosphorus: synthesis, transport properties and electronic applications. *Chem Soc Rev*. 2015;44:2732-43.
- [3] Ling X, Wang H, Huang S, Xia F, Dresselhaus MS. The renaissance of black phosphorus. *Proceedings of the National Academy of Sciences of the United States of America*. 2015;112:4523-30.
- [4] Zhang W, Huynh T, Xiu P, Zhou B, Ye C, Luan B, et al. Revealing the importance of surface morphology of nanomaterials to biological responses: Adsorption of the villin headpiece onto graphene and phosphorene. *Carbon*. 2015;94:895-902.
- [5] Sun Z, Xie H, Tang S, Yu XF, Guo Z, Shao J, et al. Ultrasmall Black Phosphorus Quantum Dots: Synthesis and Use as Photothermal Agents. *Angewandte Chemie*. 2015;54:11526-30.
- [6] Li L, Yu Y, Ye GJ, Ge Q, Ou X, Wu H, et al. Black phosphorus field-effect transistors. *Nature nanotechnology*. 2014;9:372-7.
- [7] Liu H, Neal AT, Zhu Z, Luo Z, Xu X, Tomašek D, et al. Phosphorene: An Unexplored 2D Semiconductor with a High Hole Mobility. *ACS Nano*. 2014;8:4033-41.
- [8] Im H, Huang XJ, Gu B, Choi YK. A dielectric-modulated field-effect transistor for biosensing. *Nature nanotechnology*. 2007;2:430-4.
- [9] Martinez MT, Tseng YC, Ormategui N, Loinaz I, Eritja R, Bokor J. Label-Free DNA Biosensors Based on Functionalized Carbon Nanotube Field Effect Transistors. *Nano letters*. 2009;9:530-6.
- [10] Tian B, Cohen-Karni T, Qing Q, Duan X, Xie P, Lieber CM. Three-dimensional, flexible nanoscale field-effect transistors as localized bioprobes. *Science*. 2010;329:830-4.
- [11] Kim JS, Choi JS, Lee MJ, Park BH, Bukhvalov D, Son YW, et al. Between scylla and charybdis: hydrophobic graphene-guided water diffusion on hydrophilic substrates. *Sci Rep*. 2013;3:2309.
- [12] Li Q, Song J, Besenbacher F, Dong M. Two-dimensional material confined water. *Accounts of chemical research*. 2015;48:119-27.
- [13] Peter EK, Agarwal M, Kim B, Pivkin IV, Shea JE. How water layers on graphene affect folding and adsorption of TrpZip2. *The Journal of chemical physics*. 2014;141:22D511.
- [14] Li H, Zeng X. Wetting and Interfacial Properties of Water Nanodroplets in Contact with Graphene and Monolayer Boron-Nitride Sheets. *ACS Nano*. 2012;6:2401-9.
- [15] Taherian F, Marcon V, van der Vegt NF, Leroy F. What is the contact angle of water on graphene? *Langmuir : the ACS journal of surfaces and colloids*. 2013;29:1457-65.
- [16] Li X, Li L, Wang Y, Li H, Bian X. Wetting and Interfacial Properties of Water on the Defective Graphene. *The Journal of Physical Chemistry C*. 2013;117:14106-12.
- [17] Wei N, Lv C, Xu Z. Wetting of graphene oxide: a molecular dynamics study. *Langmuir : the ACS journal of surfaces and colloids*. 2014;30:3572-8.
- [18] Chen Z, Dong L, Yang D, Lu H. Superhydrophobic graphene-based materials: surface construction and functional applications. *Advanced materials*. 2013;25:5352-9.
- [19] Gordillo MC, Marti J. Wetting and prewetting of water on top of a single sheet of hexagonal boron nitride. *Phys Rev E*. 2011;84.
- [20] Tocci G, Joly L, Michaelides A. Friction of water on graphene and hexagonal boron nitride from ab initio methods: very different slippage despite very similar interface structures. *Nano letters*. 2014;14:6872-7.

- [21] Chow PK, Singh E, Viana BC, Gao J, Luo J, Li J, et al. Wetting of Mono and Few-Layered WS₂ and MoS₂ Films Supported on SiO₂ Substrates. *ACS Nano*. 2015;9:3023-31.
- [22] Kozbial A, Gong X, Liu HT, Li L. Understanding the Intrinsic Water Wettability of Molybdenum Disulfide (MoS₂). *Langmuir : the ACS journal of surfaces and colloids*. 2015;31:8429-35.
- [23] Wei Q, Peng X. Superior mechanical flexibility of phosphorene and few-layer black phosphorus. *Appl Phys Lett*. 2014;104:251915.
- [24] Jiang JW, Park HS. Negative poisson's ratio in single-layer black phosphorus. *Nat Commun*. 2014;5.
- [25] Fei R, Yang L. Strain-engineering the anisotropic electrical conductance of few-layer black phosphorus. *Nano letters*. 2014;14:2884-9.
- [26] Hu T, Han Y, Dong J. Mechanical and electronic properties of monolayer and bilayer phosphorene under uniaxial and isotropic strains. *Nanotechnology*. 2014;25:455703.
- [27] Ge Y, Wan W, Yang F, Yao Y. The strain effect on superconductivity in phosphorene: a first-principles prediction. *New Journal of Physics*. 2015;17:035008.
- [28] Li Y, Yang S, Li J. Modulation of the electronic properties of ultrathin black phosphorus by strain and electrical field. *The Journal of Physical Chemistry C*. 2014;118:23970?6.
- [29] Cakir D, Sahin H, Peeters FM. Tuning of the electronic and optical properties of single-layer black phosphorus by strain. *Physical Review B*. 2014;90.
- [30] Mehboudi M, Utt K, Terrones H, Harriss EO, Pacheco SanJuan AA, Barraza-Lopez S. Strain and the optoelectronic properties of nonplanar phosphorene monolayers. *Proceedings of the National Academy of Sciences of the United States of America*. 2015;112:5888-92.
- [31] Qin G, Yan QB, Qin Z, Yue SY, Cui HJ, Zheng QR, et al. Hinge-like structure induced unusual properties of black phosphorus and new strategies to improve the thermoelectric performance. *Sci Rep*. 2014;4:6946.
- [32] Lv HY, Lu WJ, Shao DF, Sun YP. Enhanced thermoelectric performance of phosphorene by strain-induced band convergence. *Physical Review B*. 2014;90.
- [33] Konabe S, Yamamoto T. Significant enhancement of the thermoelectric performance of phosphorene through the application of tensile strain. *Applied Physics Express*. 2015;8:015202.
- [34] Elahi M, Khaliji K, Tabatabaei SM, Pourfath M, Asgari R. Modulation of electronic and mechanical properties of phosphorene through strain. *Physical Review B*. 2015;91.
- [35] Pronk S, Pall S, Schulz R, Larsson P, Bjelkmar P, Apostolov R, et al. GROMACS 4.5: a high-throughput and highly parallel open source molecular simulation toolkit. *Bioinformatics*. 2013;29:845-54.
- [36] Jorgensen WL, Maxwell DS, Tirado-Rives J. Development and testing of the OPLS all-atom force field on conformational energetics and properties of organic liquids. *Journal of the American Chemical Society*. 1996;118:11225-36.
- [37] Ballone P, Jones RO. A reactive force field simulation of liquid-liquid phase transitions in phosphorus. *The Journal of chemical physics*. 2004;121:8147-57.
- [38] Darden T, York D, Pedersen L. Particle mesh Ewald: An N·log(N) method for Ewald sums in large systems. *The Journal of chemical physics*. 1993;98:10089.
- [39] Bussi G, Donadio D, Parrinello M. Canonical sampling through velocity rescaling. *The Journal of chemical physics*. 2007;126:014101.
- [40] Werder T, Walther JH, Jaffe RL, Halicioglu T, Koumoutsakos P. On the Water?Carbon Interaction for Use in Molecular Dynamics Simulations of Graphite and Carbon Nanotubes. *The Journal of Physical Chemistry B*. 2003;107:1345-52.
- [41] Wang T, Li W, Liu L, Chen H, Wang Y, Zhang J, et al. The mechanism for the motion of nanoscale water droplet induced by wetting gradient: A molecular dynamic study. *Computational Materials Science*. 2015;105:39-46.
- [42] Steimel JP, Aragonés JL, Alexander-Katz A. Artificial Tribotactic Microscopic Walkers: Walking Based on Friction Gradients. *Physical Review Letters*. 2014;113.